Correlation between structure, electronic properties, and magnetism in Co_xGd_{1-x} thin amorphous films

N. Bergeard,[1,2,*] A. Mougin,[1] M. Izquierdo,[2,3] E. Fonda,[2] and F. Sirotti[2,4]

[1]*Laboratoire de Physique des Solides, CNRS, Univ. Paris-Sud, Université Paris-Saclay, 91405 Orsay Cedex, France*

[2]*Synchrotron SOLEIL, Saint Aubin, 91191 Gif sur Yvette, France*

[3]*European XFEL GmbH, Holzkoppel 4, 22869 Schenefeld, Germany*

[4]*Laboratoire de Physique de la Matière Condensèe, CNRS, Ecole Polytechnique, Université Paris-Saclay, 91128 Palaiseau, France*

(Received 10 November 2015; revised manuscript received 22 June 2017; published 14 August 2017)

Correlation between structure, electronic properties, and magnetism in Co_xGd_{1-x} thin amorphous films was investigated. The thickness averaged properties of covered thin films are consistent with those of in-depth homogeneous amorphous alloys. In spite of that, x-ray magnetic circular dichroism (XMCD) and photoemission measurements on as-grown films have shown signatures consistent with a lateral gradient composition and a Gd surfactant effect. A tendency of Gd atoms to migrate to the surface followed by an oxidation down to 8 Å has been evidenced. Our results further demonstrate the extreme sensitivity of the magnetic properties of ferrimagnetic alloys to their structure and local concentration.

DOI: 10.1103/PhysRevB.96.064418

I. INTRODUCTION

Ferrimagnetic transition metal (TM)-heavy rare-earth (RE) alloys drained a lot of investigation in the 70's due to their unique magnetic properties [1–3] that found technological application for data storage [4]. Depending on the composition of the alloys, a temperature at which the magnetization of TM sublattice compensates the magnetization of RE sublattice may exist. Such temperature is named magnetic compensation temperature (T_{comp}) [5]. A renewed interest towards those ferrimagnetic materials arose in the last decade due to their unique dynamics properties [6] as the ultrafast precessional regime in the vicinity of T_{comp} [7,8] and all-optical control of magnetization under [9] or without magnetic field [10–12]. In spite of intense experimental and theoretical effort, the processes underlying ultrafast magnetization dynamics in rare earth/transition metal alloys are still poorly understood and controversial [13–15]. Already in the bulk, all investigations pointed out the crucial importance of the TM-RE alloy composition on their magnetic properties [5]. Local composition is more important in thin films, and the growth of samples displaying the desired properties is far from trivial [16–18]. In this context, a complete structural and magnetic characterization of CoGd alloy thin films in the vicinity of the magnetic compensation temperature has been carried out.

II. SAMPLES PREPARATION

CoGd alloys were grown by co-evaporation under ultrahigh vacuum condition (P $< 2.10^{-10}$ mbar during deposition) from cells containing pure Co (99.99%) and pure Gd (99.99%) metals. The thickness and the composition of the films were tuned by the electrical power applied on each evaporator, calibrated using a quartz balance. Deposition was made at rates below 1 Å/min. The average sample composition was determined by Rutherford backscattering (RBS) measurements performed at the "group of nanometric films: Formation, interface and defaults" (CONFID) of the Institute of Nanosciences of Paris (INSP) [19]. The 10-nm-thick $Co_{0.79}Gd_{0.21}$ alloys were deposited on a SiO_2(100 nm)/Si[100] wafer and covered with a 5-nm-thick Al layer to prevent degradation in ambient atmosphere during further investigations. Those samples were used for *ex situ* characterization of the structure and magnetic properties by means of extended x-ray absorption fine structure (EXAFS, Sec. III A), magneto-optical Kerr effect (MOKE, Sec. III B), and x-ray magnetic circular dichroism (XMCD, Sec. III C), respectively.

III. CHARACTERIZATION OF CAPPED LAYERS

A. Structure determination by EXAFS

The EXAFS signals at the Gd L_3 and Co K edges have been measured at the SAMBA beam line of Synchrotron SOLEIL [20] at the surface-EXAFS station. The normalized fluorescence yield spectra for one sample of nominal composition $Co_{0.79}Gd_{0.21}$ grown at room temperature are displayed in Fig. 1. The probing depth of fluorescence detection is much larger than the alloy thickness ensuring that the average structural properties were determined. The Co K edge energy lying between the Gd L_3 and Gd L_2 edges, the Co EXAFS signal range is limited, which complicates its quantitative exploitation (Co K edge: $k = [3; 6.7]$ Å^{-1} and $r = [1.1; 3]$ Å, Gd L_3 edge: $k = [3.3; 8]$ Å^{-1} and $r = [1.1; 4.3]$ Å). For this reason, Gd L_3 and Co K EXAFS data have been jointly simulated in r space to constrain and improve the accuracy of the analysis starting from a FEFF model [21] based on the Co_5Gd structure [22]. Fourier transforms of experimental and simulated EXAFS signals are compared in Fig. 2, while the extracted parameters are listed in Table I. The refined structures of Gd and Co local environments are coherent with the starting Co_5Gd structure, but due to the limited k range available, some parameters such as Gd, Co-Gd, and Co coordination numbers have not been refined and were kept constant. All distances are related to the original Co_5Gd model by a lattice expansion factor that turns out to be 2%, thus all distances

*nicolas.bergeard@ipcms.unistra.fr

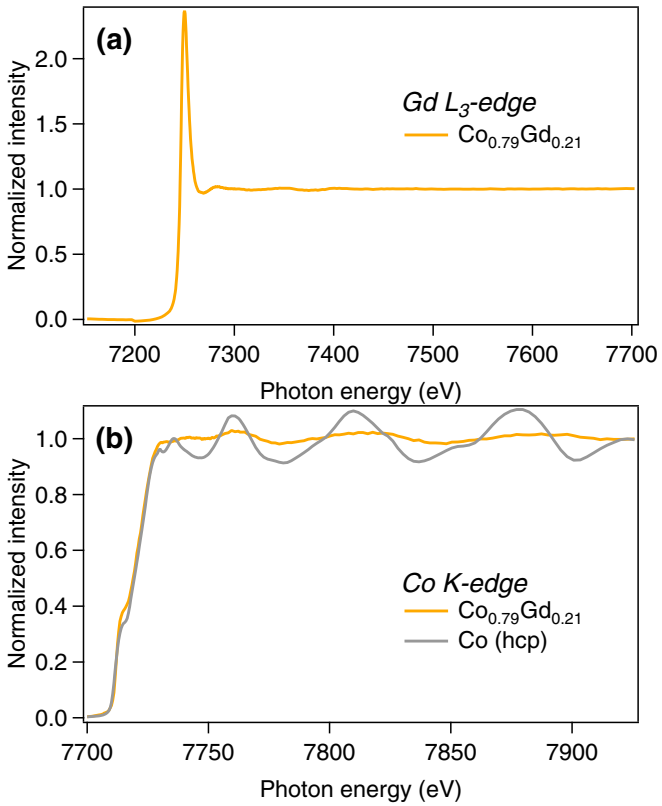

FIG. 1. X-ray absorption spectra at the L_3 edge of Gd (a) and K edge of Co (b) in the case of $Co_{0.79}Gd_{0.21}$ alloys grown at room temperature. At Co K edge, $Co_{0.79}Gd_{0.21}$ (yellow) is compared with hcp-Co (gray).

and error bars are linked. Co_5Gd contains two distinct Co sites, and this is taken into account by two different scattering paths with weighted coordination numbers (fractional values in Table I). A Gd-O contribution has also been detected and left free during the refinement. The Gd-O distance is consistent with that found in GdO bulk [23] indicating that a part of Gd has been oxidized forming GdO, in opposition

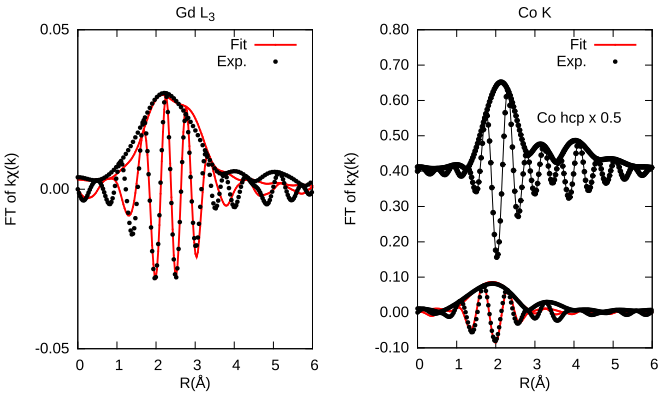

FIG. 2. Imaginary parts and moduli of Fourier transforms of experimental (black) and simulated (red) EXAFS signals measured at the Gd L_3 (left) and Co K (right) edges for $Co_{0.79}Gd_{0.21}$. At the Co edge, the Fourier transform of EXAFS signal of $Co_{0.79}Gd_{0.21}$ (bottom curve) is compared with hcp-Co (top curve).

TABLE I. EXAFS parameters obtained from FEFF simulations of Gd L_3 and Co K edge of $Co_{0.79}Gd_{0.21}$ grown at room temperature (see text for details).

Edge	Bond	N	R	σ^2 (10^{-2} Å^2)	c_3 (10^{-3} Å^3)	c_4 (10^{-4} Å^4)
Gd	Gd-O	0.7(3)	2.35(3)	0.7(2)	0.0[a]	−3(1)
Gd	Gd-Co	6[a]	2.94(2)	2.2(5)	0.0[a]	−3(1)
Co	Co-Co	4.32[a]	2.52(5)	2.7(5)	0.004(2)	0[a]
Co	Co-Co	2.16[a]	2.55(5)	2.7(5)	0.004(2)	0[a]

[a](fixed value).

with previous publications that attributed the O contribution to Gd_2O_3 [24]. On the other hand Co oxidization was not revealed by the analysis. Photoelectron spectroscopy experiments were conducted in order to determine the location of this large amount of oxygen, and results are discussed in Sec. IV. It is worth mentioning that the sample structure is extremely disordered and it has been necessary to employ a cumulant expansion model [25] for both edges. Indeed, the values for the second (σ^2), third (C_3), and fourth (C_4) cumulants, listed in Table I, differ slightly from Gd to Co, but both indicate a high degree of disorder when compared with similar studies [26]. In addition, more distant shells are undetectable which indicates a close to amorphous structure for this sample. Finally, we must notice that the proposed model is slightly poorer in Gd (16.7%) than the nominal amount (21%), which may correspond to a small Gd segregation.

B. Room temperature MOKE studies

The average magnetic properties of a 10-nm-thick $Co_{0.79}Gd_{0.21}$ alloy deposited at room temperature covered by Al 5 nm were initially characterized by MOKE [27] at the Laboratoire de Physique des Solides (Orsay). Measurements were performed at room temperature (RT) using a 620 nm (1.99 eV) laser. The thickness of the layer (10 nm ± 5 nm cover) is smaller than the penetration depth of the laser, so that the resulting magnetization curves are representative of the whole film thickness. At the wavelength used only the hybridized Co 3*d* and Gd 5*d* electronic states at the Fermi level are probed [28] with the largest signal coming from the Co 3*d* electrons [5].

The hysteresis loops of $Co_{0.79}Gd_{0.21}$ films in both longitudinal and polar configurations are displayed in Figs. 3(a) and 3(b), respectively. The results indicate an in-plane magnetic anisotropy since saturating the sample magnetization perpendicularly to the film plane requires a much larger magnetic field (around 9 kOe). From Fig. 3(a), a uniaxial in-plane magnetic anisotropy is also identified. A square loop, with a remnant magnetization of almost 100% and a coercitive field of 16 Oe, characteristic of an easy axis of magnetization, is observed in the direction perpendicular to the plane formed by the atomic flux of evaporators (sketches of Fig. 3). At 90° with respect to the easy axis of magnetization, coercitivity disappears and a magnetic field of about 200 Oe is needed to saturate the magnetization. The existence of the magnetic uniaxial in-plane anisotropy with hard magnetic direction perpendicular to the sample surface has already been observed

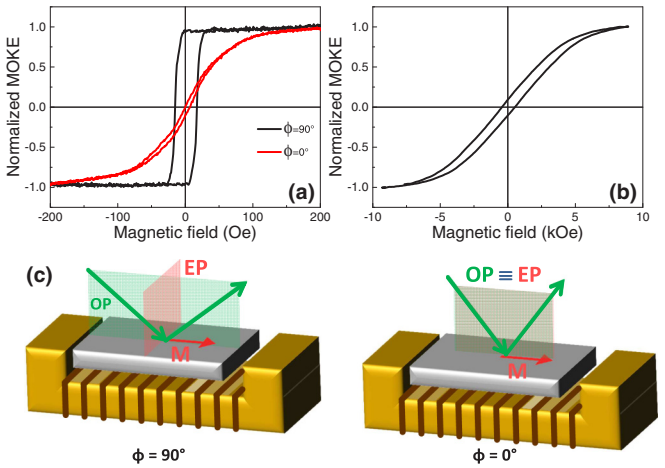

FIG. 3. (a) MOKE hysteresis loops at room temperature measured on a $Co_{0.79}Gd_{0.21}$ film acquired in longitudinal configuration, for the two orientations ($\phi = 90°$ and $0°$) defined on the sketches. (b) Hysteresis loop measured in polar configuration with the magnetic field applied along the sample normal. (c) Sketches of the experimental geometry for longitudinal MOKE configurations: For $\phi = 90°$ (left) the evaporation plane (EP) is orthogonal with the laser optical plane (OP) while for $\phi = 0°$ (right) OP and EP are co-planar.

for evaporated Co_xGd_{1-x} alloys [29] and attributed to growth shadowing effects [30].

On the one hand, the nominal $Co_{0.79}Gd_{0.21}$ alloys display on average the expected magnetic properties at room temperature such as in-plane uniaxial anisotropy as well as an amorphous and highly disordered structure. On the other hand, EXAFS measurements point towards an abnormal amount of oxygen and a slightly greater amount of cobalt that remain to be elucidated. At the nominal composition expected from the evaporation conditions, a temperature of magnetic compensation around 250 K is expected. Therefore, the thermal dependence of the Co and Gd sublattices magnetization was investigated by means of x-ray magnetic circular dichroism (XMCD).

C. Temperature dependent XMCD

XMCD technique was chosen since it gives quantitative estimation on the magnetic moments [31,32] with elemental and orbital selectivity ($3d$ for transition metals and $4f$ for rare earth [33–36]). Quantitative estimation of magnetic moments will facilitate the comparison with mean field calculations (see Sec. III C). The x-ray absorption spectroscopy (XAS) and XMCD experiments on $Co_{0.79}Gd_{0.21}$ alloys were performed at the main station of the TEMPO beamline at synchrotron SOLEIL (France) [37]. Based on the greater Co contents revealed by EXAFS measurements, the electrical power on Gd evaporator was increased to reach an alloy composition closer to the expected $Co_{0.79}Gd_{0.21}$. The soft x-rays beam (100 μm diameter) impinges the sample at an angle of 42° with respect to the sample normal. The Co $L_{2,3}$ and Gd $M_{4,5}$ absorption spectra were recorded in the total electron yield acquisition mode at remnant state after saturation of the sample magnetization with a magnetic field of 200 Oe in two opposite directions. The magnetic field was applied along

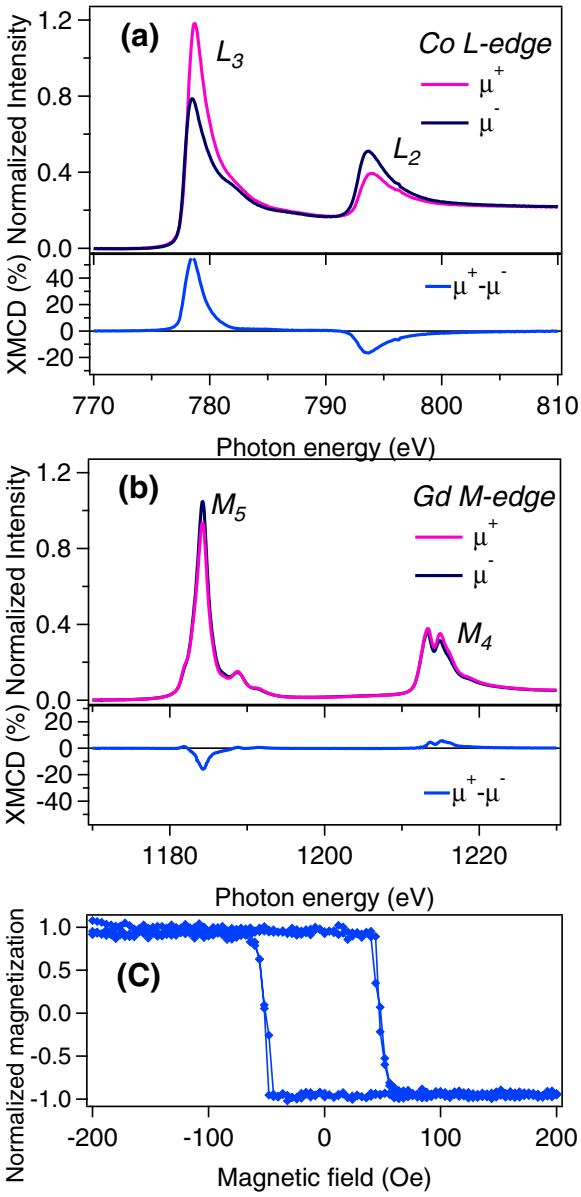

FIG. 4. [(a), top] Absorption spectra measured at the $L_{2,3}$ edges of Co in a $Co_{0.79}Gd_{0.21}$ alloy at $T = 80$ K. [(a), bottom] Dichroic spectrum at the $L_{2,3}$ edges of Co at $T = 80$ K (blue line). [(b), top] Absorption spectra measured at the $M_{4,5}$ edges of Gd in a $Co_{0.79}Gd_{0.21}$ alloy at $T = 80$ K. [(b), bottom] Dichroic spectrum at the $M_{4,5}$ edges of Gd at $T = 80$ K (blue line). For all XAS spectra, the "isotropic" XAS (i.e $\frac{\mu^- + \mu^+}{2}$) is normalized to 1 at Co L_3 and Gd M_5 edges, respectively. The XMCD spectra reported here are defined by $200*(\frac{\mu^+ - \mu^-}{\mu^- + \mu^+})$. (c) Hysteresis loop recorded by monitoring the XMCD amplitude at the Co L_3 edge as a function of the magnetic field for $T = 80$ K.

the easy axis by a horseshoe electromagnet. The hysteresis loops performed by recording the XMCD signal at the Co L_3 edge as a function of the magnetic field ensure that the samples were saturated [Fig. 4(c)]. The measurements were carried out at selected temperatures ranging from 80 K to 300 K. As an illustration, XAS and XMCD spectra recorded at $T = 80$ K for Co $L_{2,3}$ and Gd $M_{4,5}$ absorption edges are presented in Figs. 4(a) and 4(b), respectively. The Co and Gd

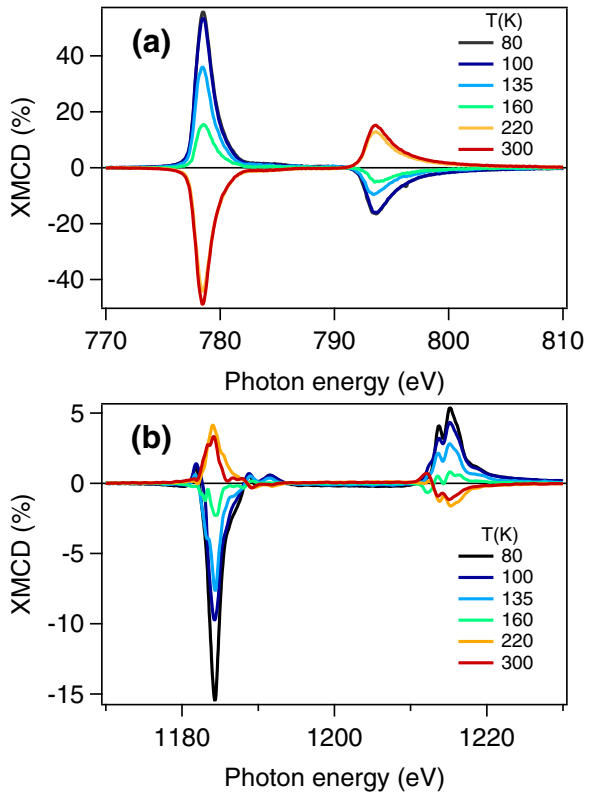

FIG. 5. XMCD spectra at the Co $L_{2,3}$ (a) and Gd $M_{4,5}$ (b) edges in a $Co_{0.79}Gd_{0.21}$ alloy at selected temperatures. Same normalization procedure as in Fig. 4 has been used.

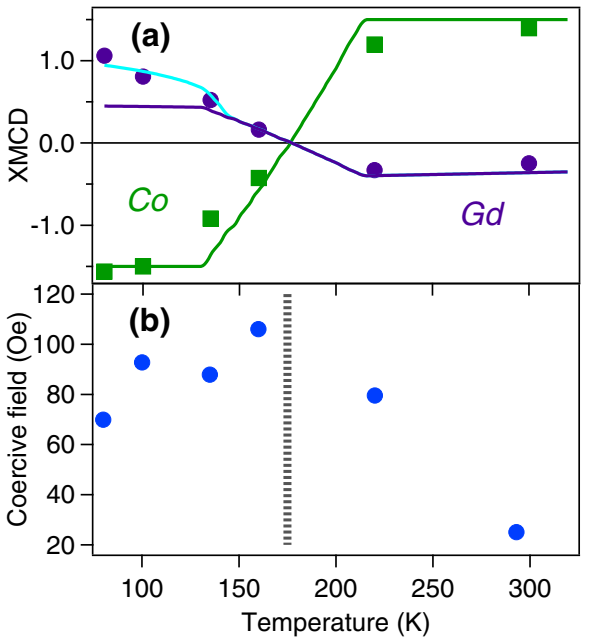

FIG. 6. (a) Magnetic moments per atom of Co (filled squares) and Gd (filled circles) derived by the sum rules analysis for a $Co_{0.79}Gd_{0.21}$ alloy at selected temperatures. The solid lines represent the mean-field calculation for Co and Gd magnetization when considering a compositional gradient (see text for details). The light blue line represents the results for the sum of the bulk and surface contribution to the Gd magnetization (see Sec. IV). (b) Coercitive field as a function of temperature extracted from XMCD hysteresis loop recorded at the Co L_3 edge. The vertical dotted line at $T = 175$ K is a rough estimation of T_{comp}.

spectra were normalized by the L_3 and M_5 edge jump of the isotropic spectra. The different XAS spectra were obtained by reversing the sample magnetization direction keeping the x-ray circular polarization fixed. The antiferromagnetic coupling of the Co and Gd sublattices is well indicated by the opposite sign of the XMCD signals at the L_3 edge of Co and at the M_5 edge of Gd [35,38]. Furthermore, the magnetization of Co sublattice points towards the opposite direction defined by the external magnetic field. The spin magnetic moment of cobalt and gadolinium atoms at $T = 80$ K were estimated to be 1.56 ± 0.1 and $1.06 \pm 0.1\ \mu_B$, respectively, by applying the sum rules analysis. For the latter derivation, the XMCD spectra were multiplied by $1/\cos(42^\circ)$ to account for the incidence of x ray. The saturation effects were also corrected following Chen's procedure by taking x-ray penetration depths of 20 and 35 nm at the Co L_3 and L_2 edges, respectively, and a escape depth of 2.5 nm for electrons [39]. It leads to 15 and 10% correction at the Co L_3 and L_2 edges, respectively. The number of holes is 2.45 following Agui *et al.* [35]. For Gd, the number of holes is 7 following Hund's rule, the penetration depth for x ray was 6.2 nm [40], and photoelectron escape depth was 1.1 nm [41].

The XMCD spectra at the Co $L_{2,3}$ and Gd $M_{4,5}$ for selected temperatures in between 80 and 300 K are plotted in Figs. 5(a) and 5(b), respectively, while the dependence of magnetic moments as a function of temperature is plotted in Fig. 6(a). The Co magnetic spin moment changes from 1.56 μ_B at 80 K to 1.39 μ_B at 300 K while the Gd magnetic spin moment decreases from 1.06 μ_B at 80 K to 0.25 μ_B at 300 K. The sign of the magnetic moment for Co and Gd is reversed when temperature is increased above $T = 160$ K indicating that the magnetic compensation is crossed in the investigated temperature range. The increase in coercive field in the vicinity of $T = 175$ K is also a clear evidence that the magnetic compensation lies around this temperature [Fig. 6(b)] [8]. Therefore, at $T < 175$ K, the Gd magnetization should be larger than Co magnetization which is inconsistent with the extremely feeble magnetic moments carried by Gd atoms [Fig. 6(a)] when compared to literature [15]. Indeed, a magnetic moment of at least 6.4 μ_B per atom is expected at this temperature and this composition in order to get a larger Gd magnetization.

D. XMCD results versus mean field calculations

In order to interpret the evolution of the magnetic properties with temperature, calculations based on the mean field theory were conducted. Mean-field calculations are known to give an accurate description of the magnetic properties of rare earth-transition metal alloys as a function of temperature [5,42]. In such calculations, the evolution of atomic magnetic moment μ_i (with i standing for RE or TM atoms) with temperature T is described using a Brillouin function for each subsystem [Eqs. (1) and (2)]. The effective magnetic field felt by the TM (H_{TM}) and RE (H_{RE}) atoms in these equations depends on

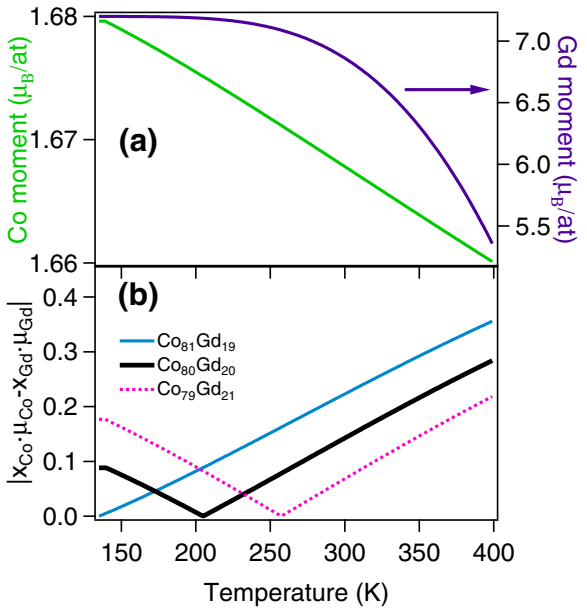

FIG. 7. (a) Calculated magnetic moments per Co and Gd atoms as a function of temperature for $Co_{0.79}Gd_{0.21}$ alloys. (b) Absolute value of the difference between the Co and Gd magnetic moments normalized by composition for $Co_{0.79}Gd_{0.21}$, $Co_{0.80}Gd_{0.20}$, and $Co_{0.81}Gd_{0.19}$ alloys.

the total momentum of the active atoms (J_i) and the Landé factor (g_i) for each species (i), as well as on the exchange coupling constant (J_{ij}) and number of nearest neighbors (Z_{ij}) [equations (3) and (4)]. In those equations, k_B and μ_B are the Boltzmann and Bohr magnetron constants. Solving the two coupled equations for μ_{TM}(T) and μ_{RE}(T), we can derive the evolution of magnetic moment with temperature of an alloy of given composition as well as that of the Co and Gd sublattices. This model was developed to obtain qualitative agreement and therefore $\mu_{Co}(0) = 1.68\ \mu_B$ and $\mu_{Gd}(0) = 7.55\ \mu_B$ were chosen. In the model, the $4f$ and $5d$ contribution to magnetic moment are not distinguished. The detail procedure is described elsewhere [43], but it is sustained by the calculated magnetic moments per atom for Co_xGd_{1-x} as a function of T for $x = 0.19, 0.2$, and 0.21 (Fig. 7) that gives a good agreement with the dependence of T_{comp} on alloy composition [29].

$$\frac{\mu_{\text{Co}}(T)}{\mu_{\text{Co}}(0)} = B_{J_{\text{Co}}}\left(\frac{\mu_{\text{Co}}(0)H_{\text{Co}}}{kT}\right) \tag{1}$$

$$\frac{\mu_{\text{Gd}}(T)}{\mu_{\text{Gd}}(0)} = B_{J_{\text{Gd}}}\left(\frac{\mu_{\text{Gd}}(0)H_{\text{Gd}}}{kT}\right) \tag{2}$$

$$H_{\text{Co}} = \frac{2J_{\text{CoCo}}Z_{\text{CoCo}}\mu_{\text{Co}}(T)}{g_{\text{Co}}^2\mu_b^2} + \frac{2J_{\text{CoGd}}Z_{\text{CoGd}}\mu_{\text{Gd}}(T)}{g_{\text{Co}}g_{\text{Gd}}\mu_b^2} \tag{3}$$

$$H_{\text{Gd}} = \frac{2J_{\text{GdGd}}Z_{\text{GdGd}}\mu_{\text{Gd}}(T)}{g_{\text{Gd}}^2\mu_b^2} + \frac{2J_{\text{CoGd}}Z_{\text{CoGd}}\mu_{\text{Co}}(T)}{g_{\text{Co}}g_{\text{Gd}}\mu_b^2} \tag{4}$$

Mean field calculations of the thermal evolution of the magnetic moments carried by Co and Gd were performed for bulk and homogeneous $Co_{0.79}Gd_{0.21}$ alloys (Fig. 7). A comparison of calculations (Fig. 7) and experimental observations (Fig. 6) raise three discordances: (i) the predicted temperature of magnetic compensation is $T = 250$ K for $x = 79\%$ [29], the nominal composition of the alloy, instead of the 175 K, (ii) the calculated Gd magnetic moments are much larger, and (iii) its variation with temperature is smoother (from 7.4 μ_B at 80 K to 6.4 μ_B at 300 K). In order to adjust the experimental temperature of magnetic compensation, the composition has to be slightly shifted towards higher Co contents as depicted in Fig. 7. Indeed, 2% shift in composition leads to a shift of about 150 K for the temperature of magnetic compensation. Therefore, the actual composition of the alloy film lies between 80 and 81% of Co, slightly above the expected value. In addition to the compositional shift, the presence of a compositional gradient in the alloy composition, distributed over the beamline spot size (100 μm) and the probed thickness has been assumed in order to reproduce the large temperature range on which the reversal occurs (solid line in Fig. 6). A 1.2% gradient modification in the sample composition, from 79.8% to 81%, is enough to reproduce qualitatively the experimental observations for Co [18,44]. This spread in the effective composition within the film thickness could be explained by partial oxidization of Gd during deposition since the evaporation rates are extremely slow (from Co 79% to apparent Co 81%, about 10% of Gd has to be oxidized). Another explanation is the existence of a compositional gradient intrinsically determined by the deposition itself [18]. Notwithstanding the origin of this gradient it is not sufficient to interpret the thermal behavior of Gd magnetic moments (solid line in Fig. 6) extracted from XMCD experiments as well as its weak magnetic moment. In the total electron yield acquisition mode, the probing depth at the Gd M_5 edge is about 1.1 nm [41] while it is about 2.5 nm for Co [39]. In the former case, the surface is probed while in the latter case, a quarter of the alloy is probed. The discrepancy of Gd (weak moments and oxidization) could then be related to interfacial properties such as the Al capping layer and/or oxidization. Therefore, investigation of the magnetic and electronic properties of uncovered CoGd alloys were performed in order to elucidate the discrepancy between experimental findings and calculations in case of Gd. To do so, surface sensitive x-ray photoelectron spectroscopy (XPS) and magnetic circular dichroism in core-level photoemission (PE-MCD) [45] were conducted.

IV. CHARACTERIZATION OF *IN SITU* DEPOSITED LAYERS

A. Surface composition

Alloys with $Co_{0.80}Gd_{0.20}$ nominal composition are investigated in this section. They were deposited at room temperature on an annealed Fe[001] monocrystal in the preparation chamber of the TEMPO beamline. The pressure in the preparation chamber was kept below 2.10^{-10} mbar during deposition and after the growth the samples were directly transferred to the XPS analysis chamber. The XPS experiments were conducted with the same geometry as for XMCD (Sec. III C). Photoelectrons were collected using a Scienta 2002 analyzer whose axis is collinear with the normal of the sample [46]. The 30 eV binding energy region below the Fermi level for the as-grown alloy is plotted in Fig. 8.

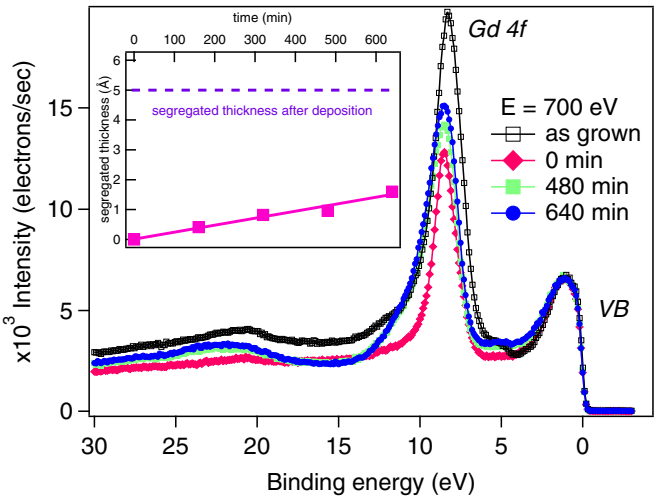

FIG. 8. XPS spectra of Co 3*d* and Gd 4*f* electrons for the as-grown $Co_{0.8}Gd_{0.2}$ sample (black squares) and after Ar sputtering (red triangles). XPS spectra for different times after sputtering are also displayed (full and empty circles). The photon energy was 700 eV and the spectra had been normalized to Co 3*d* peak intensity for quantitative comparison. (inset) Thickness of the segregate layer due to the migration of Gd atoms from the bulk towards the surface (see text). The horizontal dotted line denotes the segregated thickness measured after sample deposition.

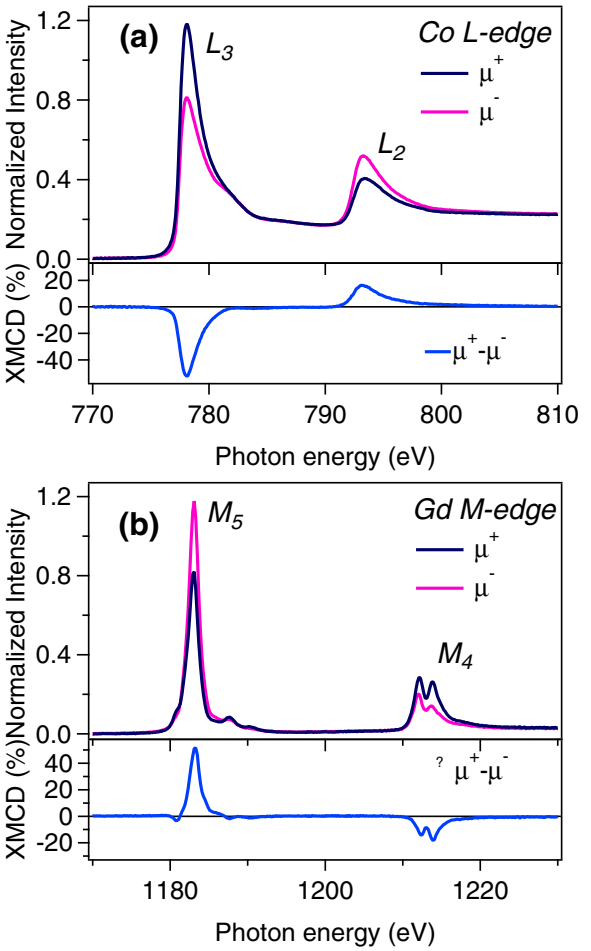

FIG. 9. [(a), top] Absorption and [(a), bottom] dichroic spectra measured at the $L_{2,3}$ edges of Co and (b) at the $M_{4,5}$ edges of Gd in a $Co_{0.80}Gd_{0.20}$ alloy at $T = 300$ K. The XMCD spectra are corrected by a factor $1/\cos(42^\circ)$ to account for the incident angle of x ray.

The main features in the spectra are the valence, with a dominant contribution of the Co 3*d* states, and the Gd 4*f*, at ∼8.6 eV binding energy. Contributions of Gd 5*d* valence electrons were neglected because its photoionization cross section is two orders of magnitude smaller than Co 3*d* at 700 eV photon energy [47]. The Gd 5*p* core level appears between 21 and 28 eV binding energy with a much lower cross section. Using the photoionization cross sections [47] and the integrated area of the Co 3*d* and the Gd 4*f* peaks a 67% Co content was derived. In order to understand the strong deviation compared to the nominal $Co_{0.80}Gd_{0.20}$ composition the sample was sputtered during 15 min with 1 KeV Ar^+ atoms in a 5×10^{-8} mbar pressure. After this treatment, the relative intensity of Gd was reduced with respect to the Co 3*d* valence band (red curve in Fig. 8). The composition of the alloy after sputtering was 81%, in agreement with the expected value from the evaporation conditions. The fact that the nominal sample composition was recovered after sputtering indicates that the films have a Gd layer at the surface. Considering that the mean free path of the Co 3*d* and Gd 4*f* photoelectrons is about 9 Å at a photon energy of 700 eV [48], the estimated thickness of this Gd layer is $d \sim 5$ Å which corresponds approximately to one Gd monolayer. During the deposition, a Gd monolayer is segregated at the surface of our alloys as previously observed [49]. According to our mean-field calculations, the Curie temperature of a gadolinium monolayer is ∼150 K, which is consistent with the broad range found in literature [50–53]. Therefore, the experimental discrepancy of Gd magnetic moment (solid line in Fig. 6) is explained by adding the contribution of the gadolinium monolayer segregated at the sample surface, as depicted by the light blue line on Fig. 6. The XMCD signal at Gd M_5 below 150 K appears as a combination of two contributions coming from the Gd in the alloy and a segregated Gd monolayer. It is worth noticing that the segregation of a Gd monolayer at the surface reduces the Gd content in the bulk, resulting in a composition slightly larger in Co than expected. This could also explain the Co composition in the bulk centered around 80.5% instead of the expected 79%. The sample measured by means of EXAFS contains less Gd which explains the larger difference between the nominal and experimental composition.

B. Room temperature XMCD

The XMCD characterization of the *in situ* deposited films was performed after removal of the Gd topmost layer (sputtered alloy). The spectra at the Co $L_{2,3}$ and the Gd $M_{4,5}$ edges [Figs. 9(a) and (b)] were recorded by using the same procedure as described in Sec. III C. The sum rules analysis gives a magnetic spin moment of $\sim1.5\ \mu_B$ for Co and $\sim3.8\mu_B$ for Gd. The noncolinear incidence of x ray with the magnetic field, and thus the magnetization, has also been corrected by a factor $1/\cos(42^\circ)$. Comparable values for Co magnetic moment have been obtained for pure Co at 300 K [54], and they are in pretty good agreement with mean field calculation

(Fig. 7) and previous experimental works based on x-ray transmission [15]. The same procedure was used to extract the spin magnetic moment in Gd. The saturation effects account for ∼10% on the XMCD signal. In this case, the Gd magnetic moment is smaller than the expected value at $T = 300$ K (6 μ_B, Fig. 7). This discrepancy between experimental and theoretical values is attributed to the surface sensitivity of total electron yield since the top Gd layer is reactive and thus subject to oxidization (see below). It should also be reminded that XMCD is sensitive to the magnetization carried by $4f$ electrons. Therefore, the experimental value misses the contribution of $5d$ electrons which is taken into account in our calculations. Nevertheless, the Gd magnetic moment in the *in situ* alloy is much larger and closer to expectation than in the case of the covered *ex situ* sample (Fig. 4). The low XMCD signal recorded at the Gd M_5 of the covered alloy is still unclear and scenarios are proposed in the following. The sign is changing at the temperature of magnetic compensation and the discrepancy of XMCD amplitude as a function of temperature proves that the magnetic signal is coming from Gd both in bulk and the segregated Gd layer (Fig. 6). The presence of nonmagnetic Gd atoms at the top of the sample would be consistent with the reduction of the XMCD signal. The XMCD amplitude at Gd M_5 for $T = 300$ K is reduced by a factor of 3 compared to the XMCD signal at the Gd M_5 edge for the uncovered $Co_{0.80}Gd_{0.20}$ films (Fig. 9). Considering an electron escape depth of 1.1 nm [41], ∼1.3 nm of nonmagnetic Gd is required to account for this reduction. According to MF calculations, the magnetization of the segregated Gd layer (0.5 nm) is zero. We also suspect that an AlGd alloy is formed during the deposition of the Al protective layer. After the deposition, a Gd monolayer is segregated towards the interface AlGd/CoGd. Further XPS analysis may sustain our claim. Some GdAl alloys such as $GdAl_2$ may present spin-glass phase at low temperature, but the XAS spectra were recorded in remnant state and therefore we do not expect magnetic contributions from this alloy [55].

The investigation of electronic and magnetic properties of $Co_{0.80}Gd_{0.20}$ alloy deposited *in situ* gave a satisfactory interpretation of the thermal dependence of the XMCD signal recorded on the *ex situ* $Co_{0.79}Gd_{0.21}$ alloys (Sec. III C). It appears that the Al capping layer and the segregation of Gd monolayers at the Al/CoGd interface strongly affect the XMCD signal at the Gd $M_{4,5}$ edges. The magnetic properties of Gd for the uncapped and sputtered CoGd alloys are consistent with the expectation for the bulk contribution. An investigation of the stability of such an alloy has been conducted.

C. Surface stability

Results presented in previous paragraphs on electronic and magnetic properties of CoGd alloys suggest the segregation of a Gd atomic layer on the deposited films. *In situ* experiments allowed us to obtain complementary information on reactivity and stability of the deposited layers. XPS spectra of the valence band for the sputtered alloy were measured as a function of time at room temperature, while the film was kept under UHV conditions ($P < 2.10^{-10}$ mbar). The results are displayed in Fig. 8 with symbols after 480 minutes (green) and 640 minutes (blue). They show an increase of the contribution of the $4f$ peak indicating a slow migration of Gd atoms from the bulk towards the surface [49]. The top Gd layer thickness estimated from the spectra is presented as a function of the time after the sputtering in the inset of Fig. 8: a migration rate of about 0.15 Å/hour (straight line in the inset of Fig. 8) was estimated. After about 1800 min (30 hours) at room temperature a Gd monolayer segregates at the sample surface. The blue dotted line in the inset of Fig. 8 indicates the thickness of the segregate Gd layer extracted from the sample measured after deposition before sputtering. Although the migration of Gd atoms towards the surface is rather slow compared to the acquisition time for static XPS and XMCD, it would become an issue for longer acquisitions, as for instance time-resolved experiments. In addition to the segregation and migration of Gd atoms, a change in the shape of the Gd $4f$ peak at a binding energy of 11 eV was also observed (see Fig. 8), indicative of oxidization of the surface Gd layer [56].

Magnetic circular dichroism in photoemission (PE-MCD) at the Co $3p$ and Gd $4d$ core levels in surface sensitive conditions was used to study the oxidization of Co and Gd as a function of time. PE-MCD signals are defined as the difference of XPS spectra recorded by reversing the relative orientation of sample magnetization and photon helicity in XMCD geometry. As for XMCD experiments, 200 Oe magnetic pulses, sufficient to saturate the magnetization, were applied in the sample plane, along the easy axis. PE-MCD signal is proportional to the sample magnetization [57]. The measuring sequence was the following: (i) the magnetization of the sample was saturated, (ii) a XPS spectrum was recorded, (iii) the magnetization of the sample was reversed, (iv) the same spectrum was recorded, and (v) the operation was repeated for another core level. For the two photon energies the acquisition started after the Ar^+ sputtering (red curve in Fig. 8) and repeated for 480 minutes, alternating between Gd $4d$ and Co $3p$.

The pressure was kept below 2.10^{-10} mbar. The XPS and PE-MCD spectra at the Co $3p$ and Gd $4d$ core levels of the $Co_{0.80}Gd_{0.20}$ film as a function of time for 700 eV photon energy are plotted in Figs. 10(a) and 10(b), respectively. The PE-MCD asymmetry is defined as the ratio between the difference and the sum of the XPS spectra measured for parallel and antiparallel directions of magnetic field and x-ray photon helicity. The maximum of the Co $3p$ PE-MCD asymmetry is constant in time indicating that the magnetic properties of Co sublattice are not modified during the measurement [49]. On the other hand, a reduction of PE-MCD signal at the Gd $4d$ core level was observed from 31% (initial value) to 13% after 360 minutes then the PE-MCD signal remains constant, which attests for a passivation of the alloy surface. The results obtained at lower photon energy (400 eV) for the Co $3p$ and Gd $4d$ core levels to enhance the signal coming from the surface are reported in Figs. 11(a) and 11(b) and 12(a) and 12(b), respectively. Again, Co $3p$ is unaffected while the asymmetry at the Gd $4d$ core level decreases from 25% to 5% within 480 minutes. The intensity of Co $3p$ XPS spectra decreases with time while it increases for Gd $4d$ which is a consequence of Gd segregation at the surface [Figs. 11(a) and 12(a)]. Except for the intensity decreases, no significant modification of the Co $3p$ peak is visible. On the contrary, for Gd $4d$, in addition to the intensity increase, a shift of the Gd $4d_{\frac{5}{2}}$ peak towards higher binding energy is visible. It is a clear indication of

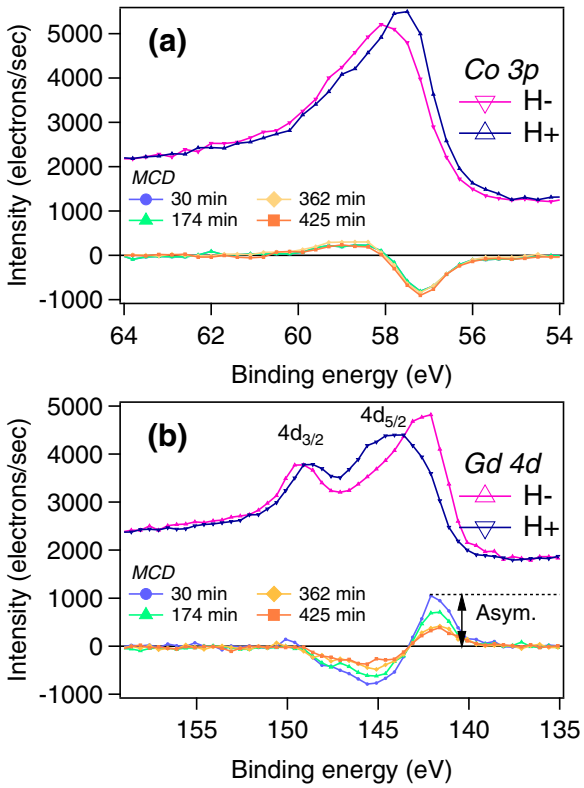

FIG. 10. [(a), top] XPS spectra of Co 3p core level for photon momentum parallel (I^+) and antiparallel (I^-) to the magnetization of the $Co_{0.8}Gd_{0.2}$ alloy. The magnetic field was 200 Oe. [(a), bottom] PE-MCD spectra, which are $I^- - I^+$, as a function of time in the UHV chamber. [(b), top] and [(b), bottom] Respectively, the same as [(a), top] and [(a), bottom] for Gd 4d core level.

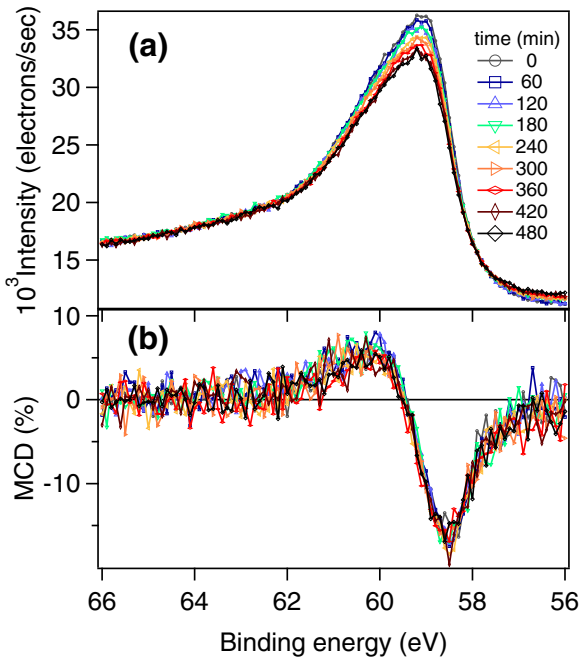

FIG. 11. [(a), top] isotropic XPS spectra of Co 3p core level of the $Co_{0.8}Gd_{0.2}$ alloy for a photon energy of 400 eV and (b) PE-MCD spectra of Co 3p as a function of time in the UHV chamber.

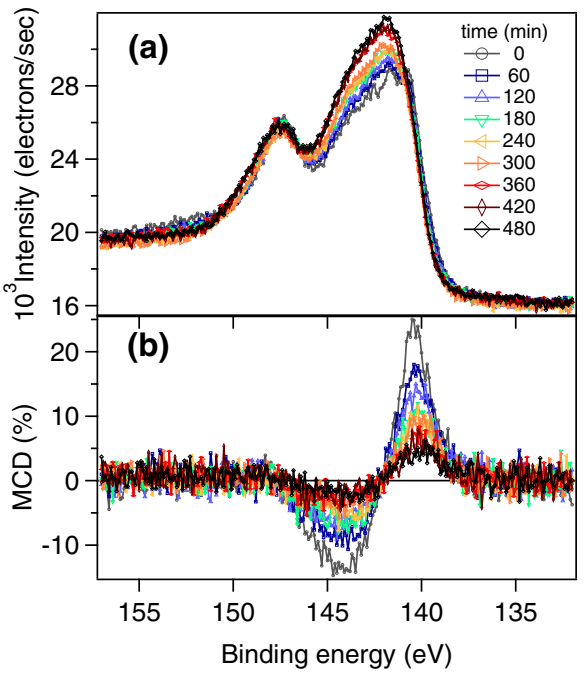

FIG. 12. [(a), top] Isotropic XPS spectra of Gd 4d core level of the $Co_{0.8}Gd_{0.2}$ alloy for a photon energy of 400 eV and (b) PE-MCD spectra of Gd 4d as a function of time in the UHV chamber.

Gd oxidization [58], and it is consistent with the decrease of PE-MCD signal. The evolution of the integrated PE-MCD spectra normalized to the initial values for Co 3p and Gd 4d core levels measured at 400 eV photon energy are plotted in Fig. 13. The MCD signal at Co 3p is almost constant within the time range investigated here, while the asymmetry at Gd 4d core level follows an exponential decay with characteristic demagnetization time of about 200 min. Those measurements show that the Gd at the surface reacts with oxygen until a saturation is reached as attested by the constant MCD signal for t > 360 min [Fig. 10(b)]. By considering the mean free path of the photoelectron, an oxidized thickness of 8 Å was estimated. Therefore, at a pressure $P < 2.10^{-10}$ mbar, the

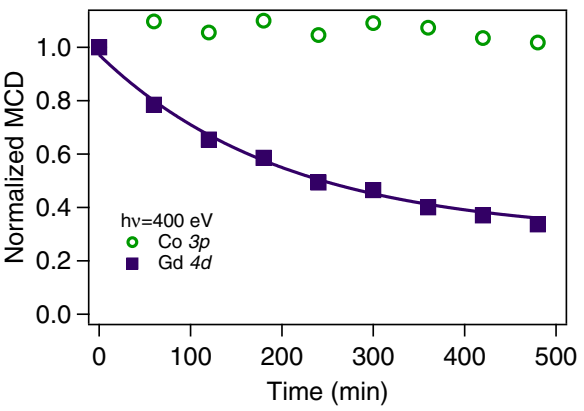

FIG. 13. MCD at the Co 3p (circles) and Gd 4d (squares) core levels as a function of time, normalized to the initial value. The photon energy was set to 400 eV. The line is an exponential fit with a characteristic time of 200 ± 20 min.

sample is protected against further oxidization while the top layers are fully oxidized. The characteristic time is 200 min which is well below the time it would take to rebuild the Gd segregated layer. The surface sensitive measurements revealed that a Gd layer always segregates at the surface and is rapidly fully oxidized and explains the low XMCD signal at the Gd M_5 edge. Moreover, the above investigation was limited to the top interface, leaving unexplored the $CoGd/SiO_2$ interface, but suggests the formation of a Gd-O layer also at the bottom interface. They also provide a source to the oxygen found in the samples investigated by EXAFS.

V. CONCLUSIONS

EXAFS, MOKE, XPS, and XMCD were used together in order to determine the structural, electronic, and magnetic properties of evaporated Co_xGd_{1-x} alloys. The alloys are amorphous and highly disordered and display in-plane uniaxial anisotropy, related to the evaporation geometry. We demonstrated that the measurements of average magnetic properties by MOKE do not reflect the complexity of the alloys morphology. Indeed, in opposition of other RE-TM alloys [59,60], we observed segregation of a Gd monolayer at the top of the sample, and we also observed a 1.2% gradient in the effective composition of the alloys distributed over the beam spot size (100 μm). We suspect that nonmagnetic AlGd alloy is formed during the deposition of the capping layer. We also estimated that the removal of the capping layer and the Gd layer segregated during the deposition is followed by a slow migration of Gd from the bulk toward the surface at a rate of approximately 0.15 Å/min and a faster oxidization of the Gd at the surface with a characteristic time of 200 ± 20 min. The sample oxidizes over 8 Å then a passivation against further oxidization is reached. Finally, we demonstrated that even under UHV conditions, the low evaporation rate induces a partial oxidization of the alloys in the bulk. The experimental investigation here does not cover the $CoGd/SiO_2$ interface at which Gd oxidization is expected and could be the major source of Gd contamination as revealed by EXAFS measurements. Extra care has to be taken concerning the morphology and the inhomogeneity of the alloys when their magnetic properties are investigated, for instance in the special case of ultrafast magnetization dynamics.

ACKNOWLEDGMENTS

N.B. was partly granted by C'NANO Ile de France (TRAM project). RBS were performed at the "group of nanometric films: Formation, interface and defaults" (CONFID) of the Institute of Nanosciences of Paris (INSP) with the help of M. d'Angelo and E. Briand. The authors are indebted to J. Ferré for MOKE experiments, A. Thiaville for the mean-field calculations, and M. Silly for support at the TEMPO beamline.

[1] P. Chaudhari, J. Cuomo, and R. Gambino, Appl. Phys. Lett. **22**, 337 (1973).
[2] A. Onton, N. Heiman, J. Suits, and W. Parrish, IBM J. Res. Dev. **20**, 409 (1976).
[3] A. Dirks and H. Leamy, J. Appl. Phys. **49**, 1735 (1978).
[4] P. Hansen, J. Magn. Magn. Mater. **83**, 6 (1990).
[5] P. Hansen, C. Clausen, G. Much, M. Rosenkranz, and K. Witter, J. Appl. Phys. **66**, 756 (1989).
[6] A. Kirilyuk, A. Kimel, and T. Rasing, Rev. Mod. Phys. **82**, 2731 (2010).
[7] C. D. Stanciu, A. V. Kimel, F. Hansteen, A. Tsukamoto, A. Itoh, A. Kiriliyuk, and T. Rasing, Phys. Rev. B **73**, 220402 (2006).
[8] M. Binder, A. Weber, O. Mosendz, G. Woltersdorf, M. Izquierdo, I. Neudecker, J. R. Dahn, T. D. Hatchard, J.-U. Thiele, C. H. Back *et al.*, Phys. Rev. B **74**, 134404 (2006).
[9] C. D. Stanciu, A. V. Kimel, F. Hansteen, A. Tsukamoto, A. Itoh, A. Kirilyuk, and Th. Rasing, Phys. Rev. Lett. **99**, 217204 (2007).
[10] C. D. Stanciu, F. Hansteen, A. V. Kimel, A. Kirilyuk, A. Tsukamoto, A. Itoh, and T. Rasing, Phys. Rev. Lett. **99**, 047601 (2007).
[11] T. A. Ostler, J. Barker, R. F. L. Evans, R. W. Chantrell, U. Atxitia, O. Chubykalo-Fesenko, S. El Moussaoui, L. Le Guyader, E. Mengotti, L. J. Heyderman *et al.*, Nat. Commun. **3**, 666 (2012).
[12] A. R. Khorsand, M. Savoini, A. Kirilyuk, A. V. Kimel, A. Tsukamoto, A. Itoh, and Th. Rasing, Phys. Rev. Lett. **108**, 127205 (2012).
[13] A. Kirilyuk, A. V. Kimel, and T. Rasing, Rep. Prog. Phys. **76**, 026501 (2013).
[14] A. J. Schellekens and B. Koopmans, Phys. Rev. B **87**, 020407 (2013).
[15] V. Lopez-Flores, N. Bergeard, V. Halte, C. Stamm, N. Pontius, M. Hehn, E. Otero, E. Beaurepaire, and C. Boeglin, Phys. Rev. B **87**, 214412 (2013).
[16] A. Hrabec, N. T. Nam, S. Pizzini, and L. Ranno, Appl. Phys. Lett. **99**, 052507 (2011).
[17] A. Mekonnen, M. Cormier, A. V. Kimel, A. Kirilyuk, A. Hrabec, L. Ranno, and T. Rasing, Phys. Rev. Lett. **107**, 117202 (2011).
[18] C. Graves, A. Reid, T. Wang, B. Wu, S. De Jong, K. Vahaplar, I. Radu, D. Bernstein, M. Messerschmidt, L. Müller *et al.*, Nat. Mater. **12**, 293 (2013).
[19] W. K. Chu, J. W. Meyer, and M. A. Nicollet, *Backscattering Spectrometry* (Academic Press, New York, 1978).
[20] V. Briois, E. Fonda, S. Belin, L. Barthe, C. La Fontaine, F. Langlois, M. Ribbens, and F. Villain SAMBA: The 4–40 keV X-ray absorption spectroscopy beamline at SOLEIL, in *UVX 2010–10e Colloque sur les Sources Cohérentes et Incohérentes UV, VUV et X: Applications et Développements Récents*, Editions de Physique (Ile de Porquerolles, 2011), p. 41.
[21] A. L. Ankudinov, B. Ravel, J. J. Rehr, and S. D. Conradson, Phys. Rev. B **58**, 7565 (1998).
[22] F. Lihl, J. R. Ehols, H. D. Wollf, and H. R. Kirchmayr, Acta Phys. Austriaca **30**, 164 (1969).
[23] S. A. Semiletov, N. A. Ragimli, and R. M. Imamov, Kristallografiya **19**, 625 (1974).
[24] J. Brunsch and A. Schneider, IEEE Trans. Magn. **13**, 1606 (1977).

[25] G. Bunker, Nucl. Instrum. Methods Phys. Res. **207**, 437 (1983).
[26] K. Machado, E. Oliveira, E. Deflon, and S. Stolf, Solid State Commun. **151**, 1280 (2011).
[27] P. N. Argyres, Phys. Rev. **97**, 334 (1955).
[28] A. R. Khorsand, M. Savoini, A. Kirilyuk, A. V. Kimel, A. Tsukamoto, A. Itoh, and T. Rasing, Phys. Rev. Lett. **110**, 107205 (2013).
[29] R. C. Taylor and A. Gangulee, J. Appl. Phys. **47**, 4666 (1976).
[30] A. Dirks and H. Leamy, Thin Solid Films **47**, 219 (1977).
[31] B. T. Thole, P. Carra, F. Sette, and G. van der Laan, Phys. Rev. Lett. **68**, 1943 (1992).
[32] P. Carra, B. T. Thole, M. Altarelli, and X. Wang, Phys. Rev. Lett. **70**, 694 (1993).
[33] S. Mangin, C. Bellouard, S. Andrieu, F. Montaigne, P. Ohresser, N. B. Brookes, and B. Barbara, Phys. Rev. B **70**, 014401 (2004).
[34] Y. Guan, Z. Dios, D. A. Arena, L. Cheng, and W. E. Bailey, J. Appl. Phys. **97**, 10A719 (2005).
[35] A. Agui, M. Mizumaki, T. Asahi, K. Matsumoto, T. Morikawa, J. Sayama, and T. Osaka, J. Phys. Chem. Solids **68**, 2148 (2007).
[36] K. Chen, D. Lott, F. Radu, F. Choueikani, E. Otero, and P. Ohresser, Phys. Rev. B **91**, 024409 (2015).
[37] F. Polack, M. Silly, C. Chauvet, B. Lagarde, N. Bergeard, M. Izquierdo, O. Chubar, D. Krizmancic, M. Ribbens, J.-P. Duval, C. Basset, S. Kubsky, and F. Sirotti, AIP Conf. Proc. **1234**, 185 (2010).
[38] M. S. S. Brooks, L. Nordstrom, and B. Johansson, J. Phys.: Condens. Matter **3**, 2357 (1991).
[39] R. Nakajima, J. Stöhr, and Y. U. Idzerda, Phys. Rev. B **59**, 6421 (1999).
[40] F. C. Vicentin, S. Turchini, F. Yubero, J. Vogel, and M. Sacchi, J. Electron Spectrosc. Relat. Phenom. **74**, 187 (1995).
[41] J. Esteva, R. Karnatak, and J. Connerade, J. Electron Spectrosc. Relat. Phenom. **31**, 1 (1983).
[42] M. Mansuripur and M. Ruane, IEEE Trans. Magn. **22**, 33 (1986).
[43] N. Bergeard, Ph.D. thesis, Universite Paris-Sud, Orsay (2010).
[44] H. Leamy and A. Dirks, J. Appl. Phys. **50**, 2871 (1979).
[45] D. Venus, Phys. Rev. B **48**, 6144 (1993).
[46] N. Bergeard, M. Silly, D. Krizmancic, C. Chauvet, M. Guzzo, J. Ricaud, M. Izquierdo, L. Stebel, P. Pittana, R. Sergo *et al.*, J. Synchrotron Radiat. **18**, 245 (2011).
[47] J. J. Yeh and I. Lindau, At. Data Nucl. Data Tables **32**, 1 (1985).
[48] I. Lindau and W. E. Spicer, J. Electron Spectrosc. Relat. Phenom. **3**, 409 (1974).
[49] D. Shen, Y. Mizokawa, H. Iwasaki, D. Shen, T. Numata, and S. Nakamura, Jpn. J. Appl. Phys. **20**, L757 (1981).
[50] M. Farle, K. Baberschke, U. Stetter, A. Aspelmeier, and F. Gerhardter, Phys. Rev. B **47**, 11571 (1993).
[51] M. Gajdzik, U. Paschen, C. Sürgers, and H. Löhneysen, Z. Phys. B: Condens. Matter **98**, 541 (1995).
[52] M. Gajdzik, T. Trappmann, C. Sürgers, and H. v. Löhneysen, Phys. Rev. B **57**, 3525 (1998).
[53] R. Kalinowski, C. Meyer, A. Wawro, and L. Baczewski, Thin Solid Films **367**, 189 (2000).
[54] C. T. Chen, Y. U. Idzerda, H.-J. Lin, N. V. Smith, G. Meigs, E. Chaban, G. H. Ho, E. Pellegrin, and F. Sette, Phys. Rev. Lett. **75**, 152 (1995).
[55] D. S. Williams, P. M. Shand, T. M. Pekarek, R. Skomski, V. Petkov, and D. L. Leslie-Pelecky, Phys. Rev. B **68**, 214404 (2003).
[56] P. Terzieff and K. Lee, J. Appl. Phys. **50**, 3565 (1979).
[57] L. Baumgarten, C. M. Schneider, H. Petersen, F. Schäfers, and J. Kirschner, Phys. Rev. Lett. **65**, 492 (1990).
[58] K. Wandelt and C. Brundle, Surf. Sci. **157**, 162 (1985).
[59] B. Hebler, A. Hassdenteufel, P. Reinhardt, H. Karl, and M. Albrecht, Front. Mater. **3**, 8 (2016).
[60] M. S. El Hadri, M. Hehn, P. Pirro, C.-H. Lambert, G. Malinowski, E. E. Fullerton, and S. Mangin, Phys. Rev. B **94**, 064419 (2016).